AD_____

AWARD NUMBER: W81XWH-12-C-0043

PRINCIPAL INVESTIGATOR: Lee Cross

CONTRACTING ORGANIZATION: Imaging Systems Technology, Inc
                           Toledo, OH 43615-3902

REPORT DATE: June 2012

TYPE OF REPORT: Final, Phase I

PREPARED FOR: U.S. Army Medical Research and Materiel Command
               Fort Detrick, Maryland 21702-5012

DISTRIBUTION STATEMENT A: Approved for Public Release;
                          Distribution Unlimited

REPORT DOCUMENTATION PAGE

Form Approved
OMB No. 0704-0188

Public reporting burden for this collection of information is estimated to average 1 hour per response, including the time for reviewing instructions, searching existing data sources, gathering and maintaining the data needed, and completing and reviewing this collection of information. Send comments regarding this burden estimate or any other aspect of this collection of information, including suggestions for reducing this burden to Department of Defense, Washington Headquarters Services, Directorate for Information Operations and Reports (0704-0188), 1215 Jefferson Davis Highway, Suite 1204, Arlington, VA 22202-4302. Respondents should be aware that notwithstanding any other provision of law, no person shall be subject to any penalty for failing to comply with a collection of information if it does not display a currently valid OMB control number. **PLEASE DO NOT RETURN YOUR FORM TO THE ABOVE ADDRESS.**

1. REPORT DATE (DD-MM-YYYY)	2. REPORT TYPE	3. DATES COVERED (From - To)
June 2012	Final ,Phase I	30 November 2011–30 June 2012

4. TITLE AND SUBTITLE

Ultraviolet Communication for Medical Applications

5a. CONTRACT NUMBER

5b. GRANT NUMBER
W81XWH-12-C-0043

5c. PROGRAM ELEMENT NUMBER

6. AUTHOR(S)
Lee Cross

5d. PROJECT NUMBER

5e. TASK NUMBER

5f. WORK UNIT NUMBER

7. PERFORMING ORGANIZATION NAME(S) AND ADDRESS(ES)

Imaging Systems Technology, Inc.
Toledo, OH 43615-3902

8. PERFORMING ORGANIZATION REPORT NUMBER

9. SPONSORING / MONITORING AGENCY NAME(S) AND ADDRESS(ES)
U.S. Army Medical Research and Materiel

Command (USAMRMC)

Fort Detrick, MD 21702-5012

10. SPONSOR/MONITOR'S ACRONYM(S)
USAMRMC

11. SPONSOR/MONITOR'S REPORT NUMBER(S)

12. DISTRIBUTION / AVAILABILITY STATEMENT
DISTRIBUTION A: Approved for Public Release; Distribution Unlimited

13. SUPPLEMENTARY NOTES

14. ABSTRACT
In this Phase I SBIR effort, Imaging Systems Technology (IST) demonstrated novel UVC-emitting Plasma-shells in a breadboard system for ultraviolet (UV) non-line-of-sight (NLOS) communication for medical battlefield casualty care. UVC Plasma-shells were fabricated and tested as optical emitter components in the solar blind 200-280 nm UVC region, and were compared with a 273 nm UV LED. A survey of state-of-the-art UVC optical components identified new devices that will make vehicle-mounted and man-portable UV NLOS systems practical by allowing power/area tradeoffs in transceiver design. A breadboard system was built to test a large-area 22 x 22 Plasma-shell transmitter panel that produced 17.6 mW optical power, with a PMT photon-counting receiver. Limited results were available from the breadboard system, however measurements of individual Plasma-shells showed emission of 12 and 24 µW at 253 and 273 nm respectively with potential for much higher output power. Ambient operating temperature was tested up to 100 °C and maximum is predicted to be 137 °C, and lifetime testing to 1050 hours shows no reduction in light output.

15. SUBJECT TERMS

16. SECURITY CLASSIFICATION OF:			17. LIMITATION OF ABSTRACT	18. NUMBER OF PAGES	19a. NAME OF RESPONSIBLE PERSON
a. REPORT Unclassified	**b. ABSTRACT** Unclassified	**c. THIS PAGE** Unclassified	UU	17	**19b. TELEPHONE NUMBER** (include area code)

Standard Form 298 (Rev. 8-98)
Prescribed by ANSI Std. 239.18

Table of Contents

Introduction

Under this Phase I SBIR, Imaging Systems Technology (IST) demonstrated that short range non-line-of-sight (NLOS) communication is possible using ultraviolet (UV) emitters and detectors in the solar-blind (SB) UVC region (200–280 nm). IST's proprietary UVC-emitting Plasma-shells are successfully demonstrated in a breadboard system. At this stage Plasma-shells are shown to compete favorably with other UVC-emitting technologies especially in cost and life.A practical direction is identified for Phase II work based on experimental results and an extensive literature review coupled with an industry survey of existing and up-and-coming devices. Phase II will incorporate best-in-class sub assemblies identified in Phase I to achieve a novel UV NLOS architecture that will extend performance well beyond published results, enabling wire replacement in battlefield medical applications.

Body

Technical Overview

Plasma-shells consist of a hollow, impervious dielectric shell of any shape that encapsulates a pressurized gas that can be ionized into plasma, as shown in Figure 1. UV phosphor in the shell produces tailored emission, and the resulting UVC spectrum is shown in Figure 2 along with the UV LED from Crystal IS used in this work. IST's proprietary manufacturing process is *extremely low cost*; Plasma-shells cost as little as $0.02 each, and can be made from a wide variety of glass, ceramic, or metallic materials. Finished sizes range from 0.5 to 10 mm, and may be filled with a variety of gases with controlled pressures from 5 to 500 Torr. Ceramic shells operate over extreme temperature ranges far greater than LEDs, and are rugged and light-weight (71 mg each).
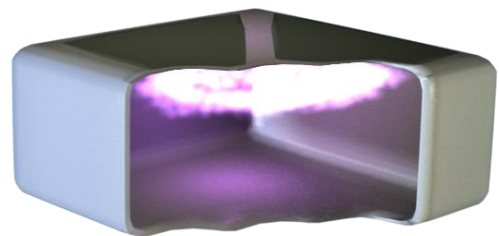

Figure 1. Plasma-shell cutaway showing internal plasma across top electrodes.
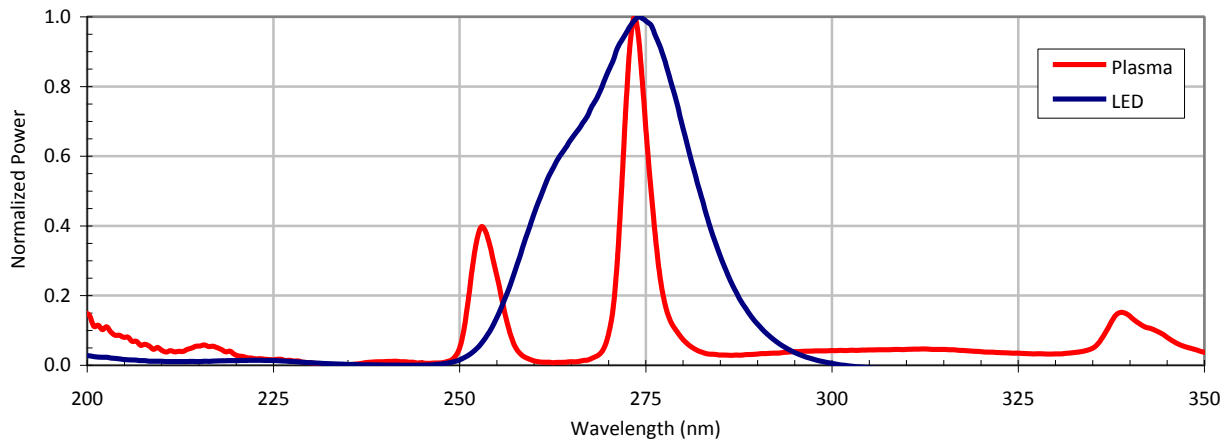
Figure 2. Normalized UVC spectra of Plasma-shell with peaks at 253 and 273 nm, and 273 nm UV LED.

This research validates the concept of UV NLOS communication envisioned in Figure 3, where Plasma-shell arrays transmit information and omni-directional detectors (spheres at corners) receive over 360°.

To support this objective, the following research tasks were carried out:

1. Survey literature and industry state of the art
2. Model NLOS communication channel
3. Improve UVC Plasma-shell
4. Investigate plasma drive waveform
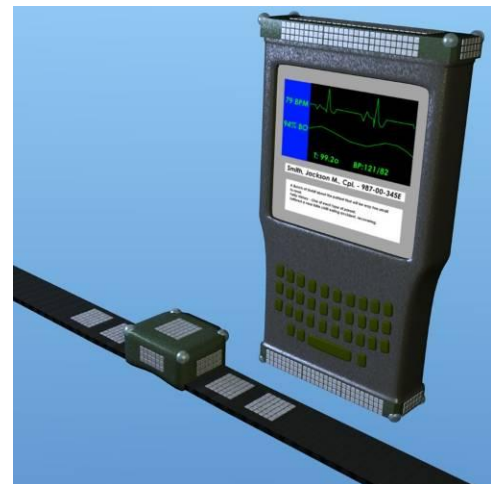5. Build breadboard system
6. Test breadboard system

Task 1: Literature Survey

Figure 3. Concept patient monitor and medic PDA with NLOS communication.

The DoD sponsored research about UV NLOS communication as far back as the 1960's, and a survey summarizing this work is included in Appendix A: Literature Review. This survey places IST's research in context of the existing body of knowledge. In brief, many UV emitters have been tested with the best candidate being recently-developed UV LED technology. IST's research introduces the novel idea of the UVC Plasma-shell emitter, a device having favorable attributes such as extreme temperature range and ultra low cost. SB receivers in literature are almost universally PMTs because of their photon counting performance and sizable active area, however size and fragility are the primary obstacles to use in a practical transceiver.

The literature survey was extended to include all commercial UV devices. In recent years, Perkin Elmer has stopped producing PMTs (some of the best available) and the remaining optical components are now owned by Excelitas. *Large-area SB detectors have been identified that will increase effective detector area by an order of magnitude* from what has been demonstrated in literature. In addition, revolutionary *miniature photon-counting devices are being introduced* that will dramatically change UV system design. IST is securing partnerships with suppliers in advance of the Phase II proposal that will present details about the devices and their use in UV NLOS systems.

Photon-counting compound semiconductor avalanche photodiodes (APD) are not yet commercially available, and no component manufacturer has stated that one is even in their new product pipeline.

Silicon APDs are sometimes used for photon counting, but often require active cooling and always have higher dark counts than PMTs. It is possible to down-convert UVC to match the spectral sensitivity of existing APDs, but this is not practical for this application because of poor quantum efficiency and stringent requirements for the SB filter.

A side-effect of the availability of both very large-area, and very compact sensors is that two different transceiver sizes may be produced: a large, high-powered uncollimated transceiver well suited to vehicles or buildings, and a much smaller low-power unit for humans or small UAVs. Asymmetrical transceiver design uses the direct trade-off between optical transmit power P_{DT} and path loss ξd^{α} (proportional to receiver area) in Equation 1 for fixed data rate (R_b, P_e), wavelength v, and distance d [2].

$$P_{DT} = \xi d^{\alpha} R_b hv \ln(2P_e)/\eta \qquad (1)$$

UV LEDs have made major advances, funded primarily for UV water purification. Crystal IS demonstrated a single LED with 9.2 mW at 260 nm, and SETi demonstrated 9.8 mW at 278 nm [1]. IST used Crystal IS LEDs in this work and plans to use more Crystal IS devices for Phase II work.

Task 2: Channel Modeling

Monte Carlo (MC) simulation is suitable for both indoor and outdoor NLOS simulation and is the standard method for accurate photon scattering simulation [2]. IST used multi scatter Monte Carlo code called "Tiny Monte Carlo" by Scott Prahl, and modified it for simple indoor and outdoor cases [4]. Modifications include:
- Wavelength-dependant atmospheric scattering
- Sender and receiver spatial distribution

Figure 4 shows an example of multi scatter MC simulation for the outdoor case, with Lambertian emitter and isotropic receiver. Functions control each photon event; launch, movement, scattering, absorption, and arrival at the receiver. MC simulations were not validated against the test bench because of hardware problems. The indoor case consisted of an opposite-facing transmitter and receiver within a rectangular enclosure, and a specular reflection function invoked when each photon reaches a boundary.
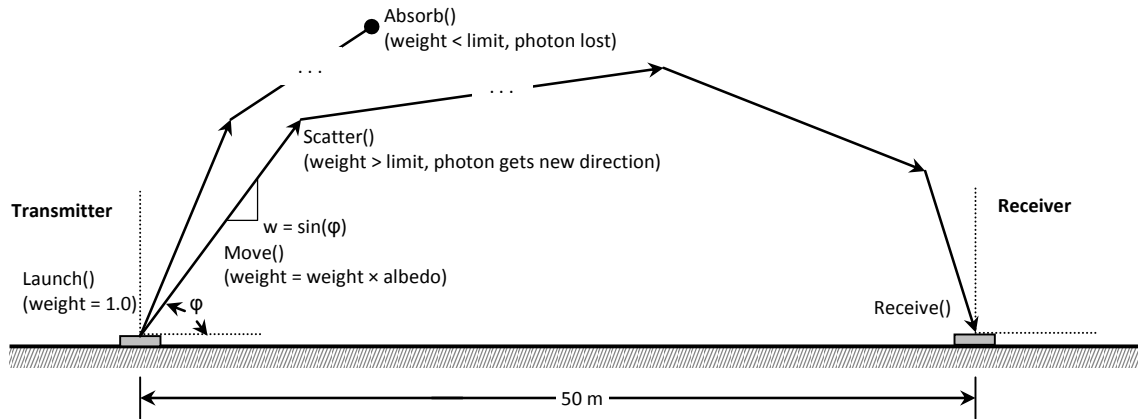

Figure 4. Example outdoor multi scatter Monte Carlo simulation.

Simulation time is long (hours on a desktop PC) because of high path loss. Use of a graphics card (GPU) processing library would dramatically reduce simulation time. Future work will use a free library called ArrayFire from AccelerEyes that wraps NVIDIA's CUDA architecture in an easy-to-use interface. This will results in several orders of magnitude reduction in simulation time for greater accuracy and exploration of design spaces.

Task 3: Plasma-shell Improvement

A series of Plasma-shell optimization experiments *increased light output by a factor of 3X*. Optimization input parameters are shell composition (phosphor loading), process temperature, shell thickness, gas mixture (xenon content), and electrode geometry. Figure 5 shows the result for each trial where first the phosphor loading was increased from 10% to 15% by weight, process temperature reduced, shell thickness slight increased, fractional xenon content doubled, and electrodes extended up the sides. Shells measure 4.4 mm × 4.4 mm × 1.8 mm, light output is measured as the total integrated optical power from 210–280 nm, and drive waveform is 100 kHz square wave at 350 V_p.

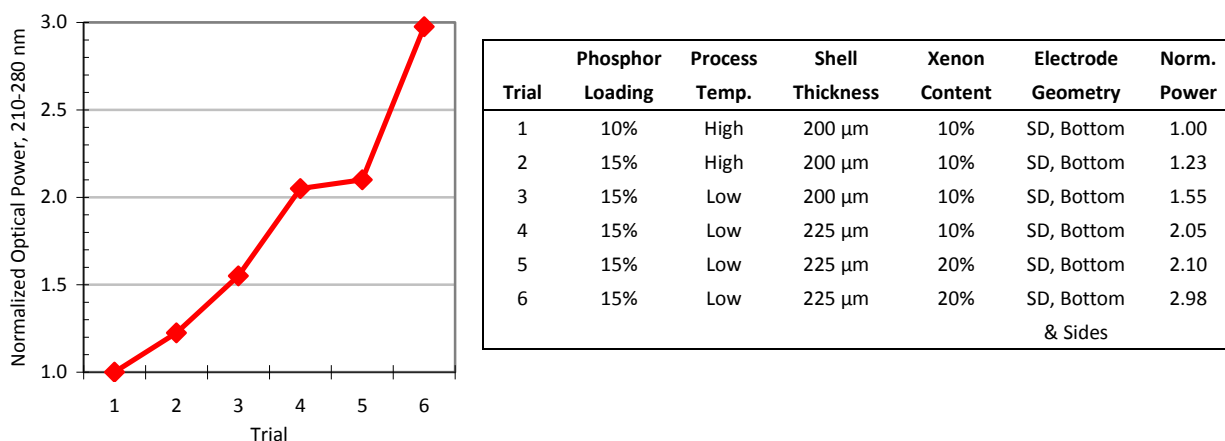| Trial	Phosphor Loading	Process Temp.	Shell Thickness	Xenon Content	Electrode Geometry	Norm. Power
1	10%	High	200 µm	10%	SD, Bottom	1.00
2	15%	High	200 µm	10%	SD, Bottom	1.23
3	15%	Low	200 µm	10%	SD, Bottom	1.55
4	15%	Low	225 µm	10%	SD, Bottom	2.05
5	15%	Low	225 µm	20%	SD, Bottom	2.10
6	15%	Low	225 µm	20%	SD, Bottom & Sides	2.98

Figure 5. Process improvements increase power output by *factor of 3X*.

There is considerable potential to increase light emission further. First, *doubling shell height will double light output*. The very first manufacturing run for this project produced a 4.5 mm × 4.5 mm × 4.0 mm shell with the same parameters as Trial 1 and was electroded up the sides, producing 12.8 µW. This shape has yield problems, so the lower height was used instead for the optimization experiment. Had the shell in Trial 1 been electroded up the sides, emission would be 42% higher (Trial 6 divided by Trial 5), increasing measured power to 5.7 µW. Therefore, increasing height from 1.8 to 4.0 mm would increase light output by *a factor of 2.25X*.

Second, different shell materials can increase light output by a *factor of 6X*. Measured shell transmissivity is 15% at 254 nm and 50% in

Figure 6. Highly transmissive Schott glass enables *6X improvement*, source Schott product literature.

visible, meaning transmissivity rolls off in UV and a majority of UV energy is blocked by the shell. Highly transmissive materials such as Schott glass 8337B and 8405 shown in Figure 6 shows 90% transmissivity at 270 nm. Cursory trials with silicon dioxide (SiO_2) and magnesium aluminum oxide (spinel) did not produce lighting shells, but further research is warranted with all these materials.
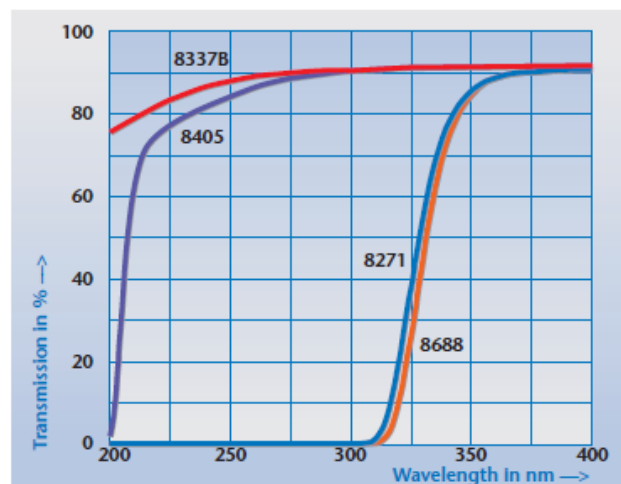
Finally, optimal results will be achieved with a full optimization of each shell parameter rather than a binary selection of optimization parameter values. Other degrees of freedom should be explored including shape and size, new phosphors, shell layering, and processing profiles.

Task 4: Drive Waveform

Plasma-shells are voltage-controlled devices and the applied voltage waveform substantially effects light output. Optimized UV Plasma-shells developed in the previous task were tested with three different waveforms: 100 kHz square wave, 1 MHz sine wave, and 900 MHz sine wave. Highest UVC output was attained with the conventional 100 kHz square wave.

The 100 kHz square wave is the most common drive waveform for plasma displays. Figure 7 shows the effect of changing drive voltage for the breadboard emitter panel. Panel UV power density, measured with a calibrated Ocean Optics Jaz spectrometer with Spectralon cosine corrector, increases by a factor of 2X as drive voltage increases from 300 to 600 V_p, and the plateau suggests a sweet spot at 450 V_p as a compromise between drive voltage and power output.
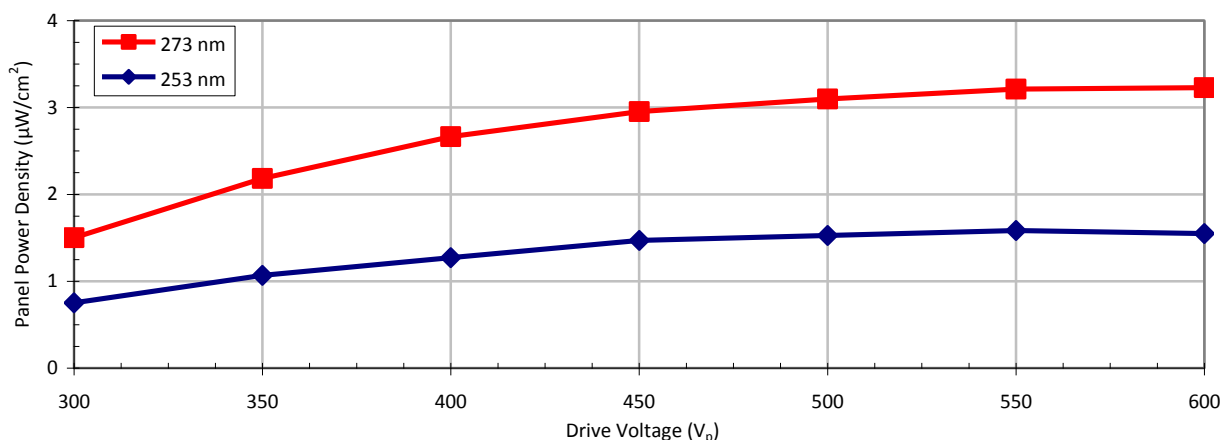

Figure 7. Breadboard panel power density versus drive voltage, 5 kHz square wave.

Higher drive frequency allows more drive energy to couple to the plasma through the shell reactance, and as frequency approaches 1 MHz the plasma becomes continuous. Using IST's 1 MHz drive electronics to supply 650 V_p, and a custom split ring resonator PCB for 900 MHz sustaining at 400 W, neither approach increased UV emission. At 1 MHz, neon atoms are more involved in emission and power dissipation is very high. At 900 MHz, xenon atoms dominate the plasma emission spectrum yet UVC output was lower than 100 kHz, and shell temperature rise was excessive. Emission spectra showed xenon emission peaks much higher when excited at 900 MHz, particularly at 470 and 760 nm, however this did not translate to higher vacuum UV (VUV) emission that would increase UVC phosphor emission.

Task 5: Build Breadboard System

The UV NLOS communication channel is tested with a breadboard system composed of IST's Plasma-shell emitter panel and IST's inventory of optical equipment and drive electronics. Figure 8 shows the breadboard system block diagram that generates short optical pulses with either an LED or Plasma-shell source, and receives scattered photons with a photon-counting PMT and data-logs the received photon-count-versus-time output onto a memory card for later analysis. Note that filters and optics were omitted during testing because of significant attenuation and a faulty PMT/base that degraded sensitivity.
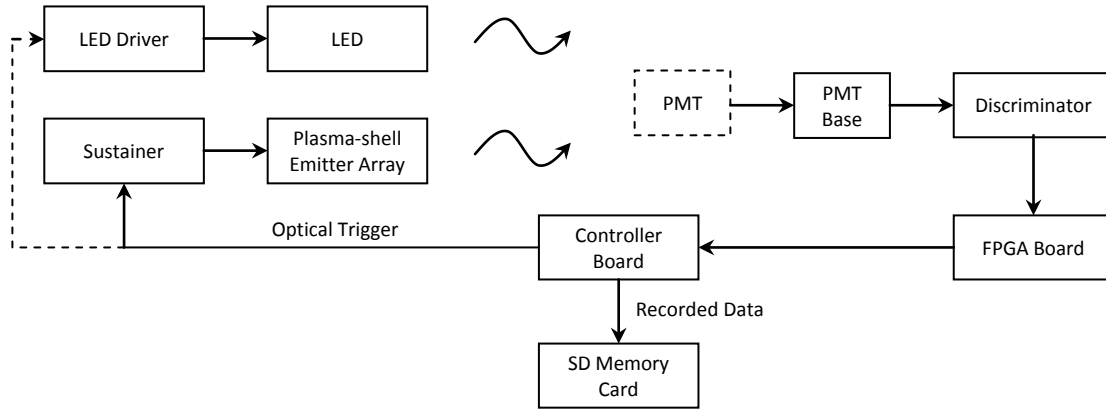
Figure 8. Breadboard system block diagram.

The receiver is a Hamamatsu R7154 PMT with SB photocathode that is ideal for photon counting, used with a C8991 or C8728 socket base. Active area is 8 mm × 24 mm, quantum efficiency is 20% at 270 nm, and dark count is extremely low. A custom wide-angle lens was manufactured by Light Works for this work that includes an enclosure and removable filter. Single-crystal solar blind filters provide exceptional rejection but are extremely expensive, ruling out the Ofil filters SB-AF-1 and SB-270-1. Instead, conventional absorptive/dielectric stack filters were ordered from Edmunds Optics: NT67-812 for 270 nm and NT67-808 for 254 nm. The Hamamatsu C9744 discriminator converts narrow PMT pulses to a TTL pulse stream, and custom IST FPGA and microcontroller boards captured the digital signals and saved them to a SD card.

The sources shown in Figure 9 are the 22 × 22 Plasma-shell array fabricated using the optimized shells described in Task 3, and one heat-sink-mounted Crystal IS 273 nm UV LED, rated at 2.593 mW at 100 mA.
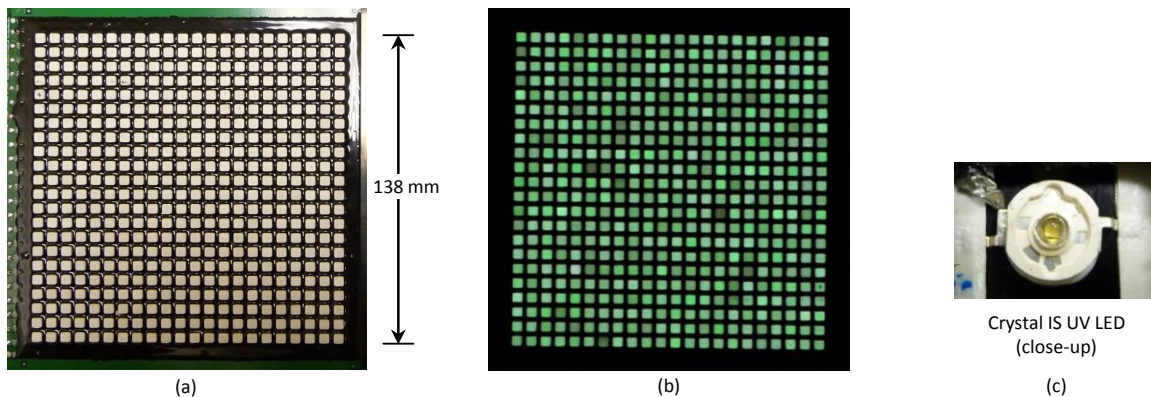

Figure 9. UVC emitters: (a) fabricated 22 × 22 Plasma-shell array off and (b) on, and (c) 273 nm UV LED.

The Plasma-shell emitter panel was sustained with a 5 kHz square wave, which produces plasma discharges every 100 µs. The location of each discharge can be modulated to produce M-ary pulse position modulation (PPM), which encodes multiple bits of data onto each pulse. In this way, data rates exceeding 57.6 kbps are possible.

Panel brightness measures 4.6 µW/cm^2 with the cosine corrector 2 cm from the surface and brightness can be doubled if shells are placed edge-to-edge rather than on 6.35 mm centers. Maximum continuous (CW) power of the panel is 17.6 mW when driven at 100 kHz, with each shell emitting 36 µW.

Crystal IS did not provide the maximum safe value for pulse current, so the maximum CW current of 100 mA was used for pulsed experiments. Rated optical output power is 2.593 mW, and this power level was verified by IST within 20% with the calibrated Jaz spectrometer.

Task 6: Test Breadboard System

This task demonstrates principles and performance of UV NLOS communication. In addition, performance data was supposed to be used to validate MC modeling. However, the PMT receiver showed sensitivity far below the datasheet specification, and the test setup was unable to demonstrate data transmission performance. Even with degraded performance, some measurements were still possible. Figure 10 shows a received photon count waveform of a single Plasma-shell sustain emission with all optics and filters in place and short line-of-sight (LOS) path from sender to receiver. The waveform shows the expected double exponent profile, where the fast rising edge corresponds to the single fast-rising plasma emission and the decay trailing edge is indicative of phosphor persistence with time constant 7.5 µs, which is suitable for high data rate communication.
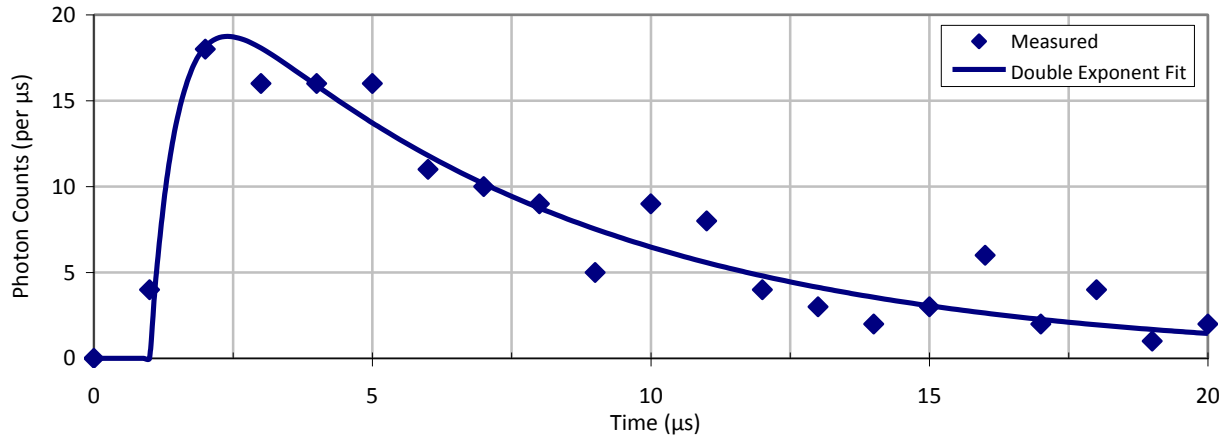

Figure 10. Plasma-shell single pulse emission profile recorded by breadboard system.

The experimental setup in Figure 11 was used to measure attenuation of each receiver optical component by successively removing each component between the LED and PMT and adjusting LED current to hold the received photon count f_c constant at 2.5 MHz. With low LED forward current, optical power is proportional to current, and discriminator nonlinearity can be ignored for constant count rates. For reference, LED output power reported by the manufacturer is 411 µW at 20 mA.
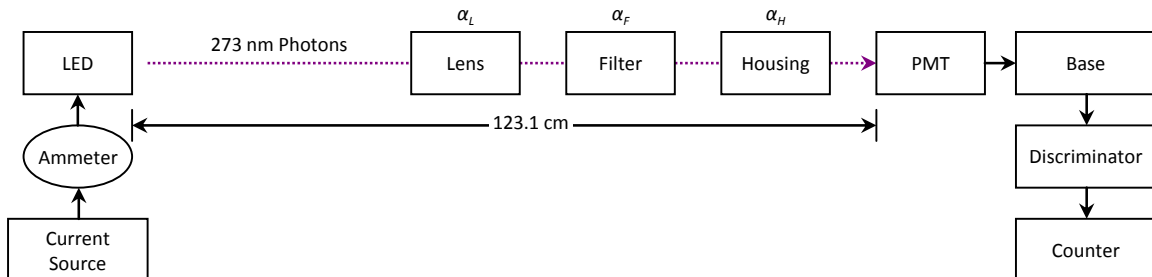

Figure 11. Optical component attenuation measurement setup.

Using forward LED current to calculate the attenuation constant of each optical component, Table 1 shows that the housing covers 30% of the PMT active area. The lens converts the PMT active area into an isotropic receiver, which reduces the apparent entrance pupil while maintaining receiver effective

area over the entire field of view. While this is not attenuation in the strict sense, it is accounted as such for simple calculation. There is also a component of attenuation from lens losses that is not considered. Finally, filter bandwidth was selected for the UVC phosphor so is too narrow for the LED spectrum and blocks at least half the out-of-band energy and attenuates within the passband. Because of high optical component attenuation and defective PMT sensitivity, outdoor NLOS testing was conducted without any optics.

Table 1. Optical component attenuation.

Configuration	LED Current (mA)	Attenuation Constant (dB)
PMT	0.60	
PMT + Housing	0.86	α_H = 1.6
PMT + Housing + Lens	6.97	α_L = 9.1
PMT + Housing + Lens + Filter	45.00	α_F = 8.1

Investigating the poor PMT sensitivity, the culprit was isolated to either the PMT or base. Long lead time prevented replacement before the end of the project. Calculating the PMT sensitivity deviation from first principles (see Appendix B: PMT Sensitivity), sensitivity is degraded by 19 dB, limiting range.

The breadboard system was tested outdoors at midnight on a clear cloudless night. The building flood lights were all turned off, however street lights, while not LOS, cast light on objects surrounding the parking lot. Because the test was conducted without SB filters, ambient UVA and UVB levels that are not entirely rejected by the PMT SB photocathode, measured 40 counts per 20 µs. This is a very high noise value for a photon counting system, so averaging was used to improve the signal to noise ratio (SNR) for the single repetitive pulses used. This would not be a problem with a SB filter or darker surroundings.

An average of ten received pulses are shown in Figure 12 for the Plasma-shell emitter panel, and the single 273 nm LED is pulsed on for 10 µs at 100 mA and is indistinguishable.
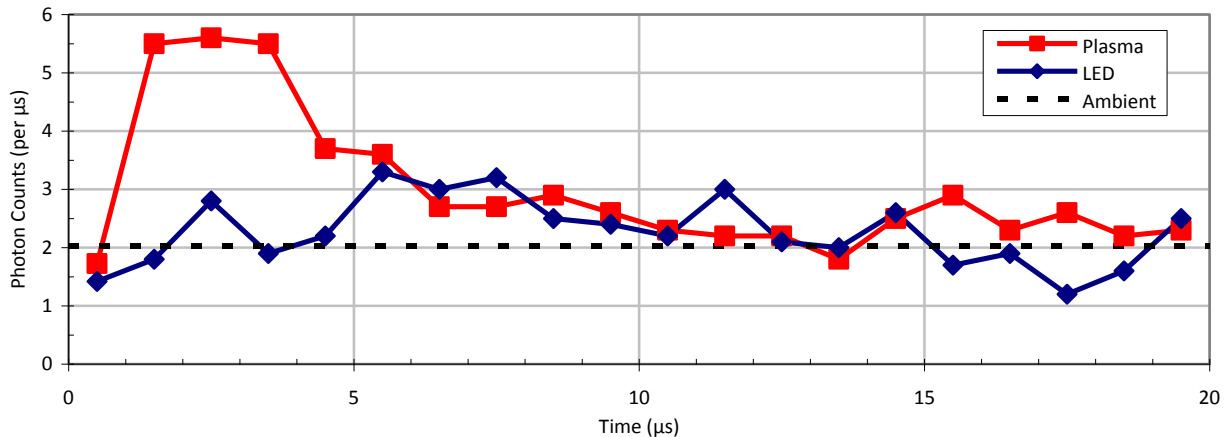

Figure 12. Received photons, 2.2 m distance, for Plasma-shell panel and LED emitters.

Beyond this distance, ambient noise counts were too high to resolve single pulses from time-domain data. In Figure 13, it is clear that the UV LED power is insufficient and only the shortest distance contributes measurable photon counts. The Plasma-shell panel has considerably more power and shows evidence of a linear power-distance relationship, although the received photon count is barely detectable at the maximum tested distance of 15 m.
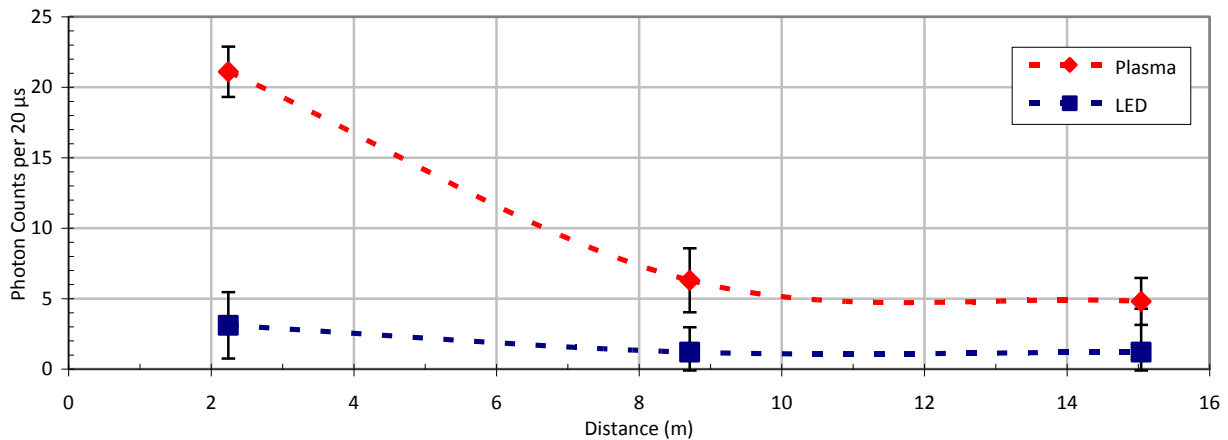
Figure 13. Single pulse received photon counts at three distances, with ambient counts removed.

Unfortunately communication performance cannot be tested with this system; range is too short and ambient noise is too high, however it does demonstrate that use of uncollimated optics is possible.

Plasma-shell Advantages

UVC Plasma-shells will increase brightness by more than an order of magnitude with further development. Since Plasma-shells were first developed for color displays in 2005, brightness has dramatically increased by almost *two orders of magnitude* and continues. Figure 14 shows the current state of the art for green shells, and UVC Plasma-shells are following a steeper trajectory by demonstrating 3X improvement in this work, and another order of magnitude within reach.
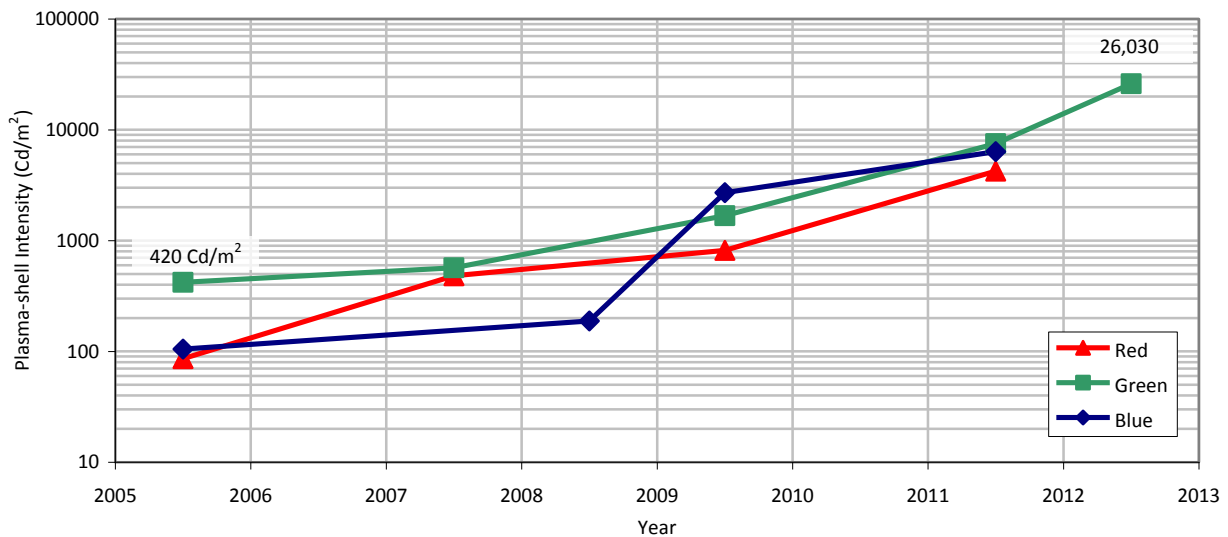

Figure 14. Plasma-shell visible light intensity improvement since 2005.

Plasma-shells have excellent lifetime. Green Plasma-shells have demonstrated lifetime to 50% power exceeding 20,000 hours at 100% duty cycle, and the UVC Plasma-shells developed in this work are showing very promising lifetime data as well. Figure 15 shows the average output of three UVC shells normalized to burn-in time of 24 hours, with mildly increasing power output to the end of this research period at 1050 hours. This experiment is ongoing to provide important lifetime data, and already shows

favorable comparison to UVC LEDs with lifetime as short as 1000 hours, and environmentally-toxic mercury lamps with lifetime less than 10,000 hours [5].
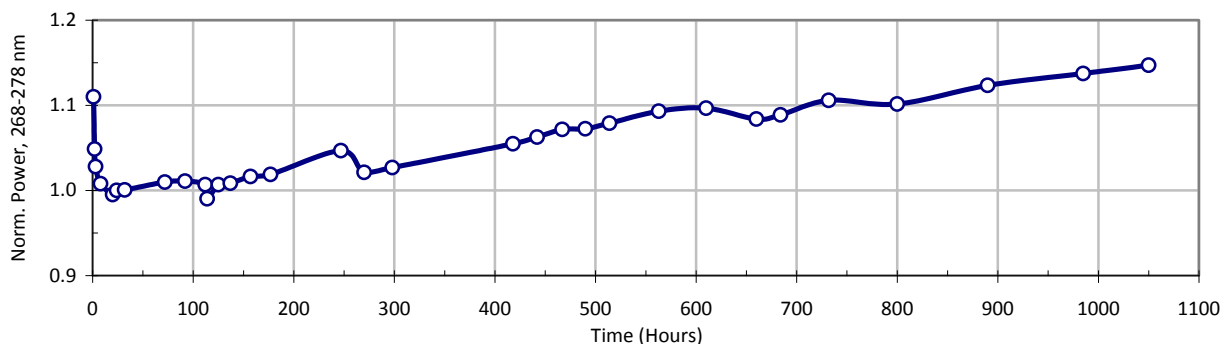

Figure 15. Plasma-shell output power normalized to 24 hours is steady to 1050 hours.

Plasma-shells have extreme operating temperature range. Figure 16 shows optical power output normalized to room temperature, measured up to 100 °C (maximum temperature for spectrometer integrating head). Light output declines to 75% at 100 °C, and a curve fit predicts 50% power at *137 °C*, far higher than any semiconductor light source. For example, a typical 270 nm LED from SETi outputs 50% power at less than 60 °C [6]. This is an important factor for all-climate operation, such as deserts where surfaces can get as hot as 80 °C. In addition, Plasma-shells do not require any special heat sinking, a costly and critical requirement for high-power LEDs.
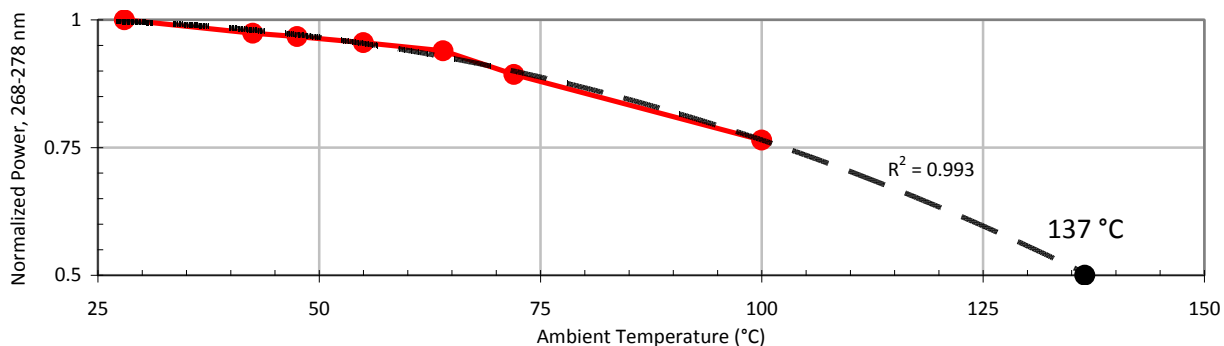

Figure 16. Plasma-shell output power versus temperature predicts 137 °C maximum temperature.

Plasma-shells are extremely low cost. The bulk manufacturing process yields tens of thousands of Plasma-shells per run, with cost as low as $0.02 per shell in volume. Table 2 cost projection are order of magnitude lower with improvements such as doubled power from taller shells and factor of six more power from high-transmissivity shell material, versus the Crystal IS LED used in this work (using cost data from 270 nm SETi LED, qty 1,000,000 [7]) that cannot currently be mass produced.

Table 2. High-volume price/performance of Plasma-shells with improved performance versus UV LED.

	Plasma-shell			UV LED
	This Work	**2X Height**	**6X Transmissivity**	
Device Cost ($)	$0.02	$0.02	$0.02	$7.95
Output (mW)	0.037	0.074	0.444	2.593
Cost ($/mW)	$0.54	$0.27	*$0.05*	**$3.07**

Safety

Safety is an important consideration when working with deep UV sources. Safe exposure limits for eyes and skin are defined differently in sources; one source defines the maximum effective dose for the general population to be 3.0 mJ/cm^2 over an 8 hour work period, where the effective dose is weighted to the most sensitive wavelength of 270 nm (the primary wavelength used in this work), and 254 nm is exactly half sensitivity (twice the permitted dose) [8]. Another source limits continuous exposure to 0.1 µW/cm^2 irradiance [9]. Finally, a higher dose of 0.5 µW/cm^2 is permitted over a 7 hour period [10].

Plasma-shells are inherently much safer than high-power LEDs; the distributed Lambertian source will have many orders of magnitude lower power density than focused high power LEDs when near the source. Even so, human exposure should be limited by minimizing transmitter duty cycle (low power coding, compression) and maximizing distance to skin and eyes. Plasma-shells used in this work are capable of delivering a maximum dose in less than one minute if operated at maximum output.

Key Research Accomplishments

- Created UVC-emitting Plasma-shell
  - Demonstrated extreme temperature range (137 °C)
  - Demonstrated lifetime exceeding 1000 hours (and counting)
  - Increased output power by factor of 3X, to 36 µW per device
    - Increase by factor of 2X is immediately feasible
  - Manufactured large emitter panel, 17.6 mW total
    - Larger panels are immediately feasible
- Demonstrated pulse transmission with uncollimated optics
- Indentified photon-counting detectors with very large-area, and compact form factor
  - Established relationship with UVC device manufacturers
- Proposed new UV NLOS communication configuration
  - Asymmetric transceivers: large fixed transceivers, small mobile transceivers
- Implemented Monte Carlo photon scattering code for simulation

Reportable Outcomes

- Submitted **Phase I SBIR proposal** for NSF topic EI/ED1 (Electronics, Information and Communication Technologies: Optoelectronic Devices), "UV Plasma-Shell Device for Novel Photocatalytic Process," 6/19/2012.
  - Proposes UVA and UVC Plasma-shells (developed in this work) for use in water purification, with outer layer of titanium dioxide photocatalyst.
- Presented **conference poster** at American Water Works Assn. ACE12, "Use of Plasma-shell Technology for Concurrent Control of Chemical and Microbial Waterborne Contaminates," Dallas, TX, 6/13/2012.
  - Co-written by Dr. Audrey Levine (Battelle), and Dr. Adeline Meirmont, Carol Wedding, and Vicki Kurtz of IST. Discusses UVA and UVC Plasma-shells (developed in this work) for chemical and biological neutralization of potable water.
- Presented **conference poster** at Making Water Connections 2012 Water Technology Innovation Cluster Conference, "Water Purification with IST Plasma-Shells," Dayton, OH, 5/22/2012.
- Upcoming **conference poster** presentation at the International Ultra-Violet Association (IUVA) conference, "Moving Forward: Sustainable UV Solutions to Meet Evolving Regulatory Challenges," Washington, DC, 8/12/2012.

Conclusion

Plasma-shells provide pulsed UVC emission suitable for UV NLOS communication. They are currently available in large quantities at very low price to enable conformal, low-profile transmitter panels that do not require aiming. Initial UVC Plasma-shells demonstrated power improvement by a factor of 3X to 36 µW per device, and will be improved by more than an order of magnitude. This enables high-power panels that operate at extreme temperature ranges (> 130 °C) at an order-of-magnitude lower price. Preliminary lifetime testing out to 1050 hours shows no power drop whatsoever, implying excellent life.

Extremely large-area photon-counting receivers have also been identified, which enable order-of-magnitude more sensitive detectors. The concept of asymmetrical transceivers is proposed, where large transceivers are used on fixed installations such as vehicles, and compact/low-power transceivers for humans and small unmanned vehicles. Plasma-shells are ideal for the concept shown in Figure 17 of a high-power transceiver susceptible to temperature extremes outside a medevac helicopter.

Figure 17. Concept of conformal Plasma-shell transceiver panel with large-area (a) detector and (b) emitter array, providing high-power 360° coverage for vehicles in a low-profile, light-weight package.

A breadboard system demonstrated a very large Plasma-shell panel emitting up to 17.6 mW at 253 and 273 nm. Unfortunately a defective PMT prevented practical data communication and validation of the customized Monte Carlo simulation code. Omni-directional optics were built and tested, however lower path loss and smaller volume will be achieved by using large-area, low-profile sensors with only solar blind filters. IST will continue working with both UV LEDs and UV Plasma-shell technology, believing that both technologies have distinct advantages for different transceiver designs.

References

[1] (2012) *New Efficiency Record for Germicidal UV LEDs* [Online]. Available: http://optics.org/news/3/4/26

[2] Q. He, Z. Xu, B. M. Sadler, "Non-Line-Of-Sight Serial Relayed Link for Optical Wireless

Communications," *Mil. Comms. Conf.*, 2010.

[3]   L. H. Wang, S. L. Jacques, L. Q. Zheng, "Convolution for Responses to a Finite Diameter Photon Beam Incident on Multi-Layered Tissues," *Comp. Methods and Prog. In Bio. Med.*, vol. 54, pp. 141-150, 1997.

[4]   (2012) S. Prahl, "Drop-Dead Simple Monte Carlo Codes," [Online]. Available: http://omlc.ogi.edu/software/mc

[5]   C. Chatterley, K. Linden, "Demonstration and Evaluation of Germicidal UV-LEDs for Point-of-Use Water Disinfection," *J. Water and Health*, 2010.

[6]   (2012) *UVTOP Deep UV LED Technical Catalogue* [Online]. Available: http://www.s-et.com/uvtop-catalogue.pdf

[7]   (2012) *UVTOP Price List* [Online]. Available: http://www.s-et.com/price-list.pdf

[8]   Guidelines on Limits of Exposure to Ultraviolet Radiation of Wavelengths between 180 nm and 400 nm (Incoherent Optical Radiation), International Commission on Non-Ionizing Radiation Protection*, Health Phys*, 71:978, 2004.

[9]   Standard: IEC 60825-12:2005, Safety of Laser Products–Part 12: Safety of Free Space Optical Communication Systems used for Transmission of Information.

[10] L. R. Koller, *Ultraviolet Radiation*, 2nd ed., John Wiley & Sons, New York, 1965.

Appendix A: Literature Review

A summary of the referenced sources were reviewed to help determine the current state of the art for NLOS solar blind UV communications systems. The concept of NLOS UV communications in the solar blind UV region from 200-290 nm was first proposed in 1968. The advantages of being non-line-of-site, covert, and quantum-limited as opposed to background-limited are universally recognized throughout all the listed sources.

The fields of study include research into UV emitter technology, UV receiver technology, NLOS path modeling, and development of communications protocols that are tolerant of NLOS UV communications. The protocol-oriented papers [12, 15] are not particularly relevant to this phase of study.

Path modeling studies have used Monte Carlo analysis and stochiometric methods to produce results that agree well with measured data.

UV receiver technology is primarily based on Photo Multiplier Tubes (PMTs) [A-7, A-10]. PMTs have the advantage of extreme sensitivity (can detect single photons); low-dark counts, and are sensitive in the solar-blind region. However, being tube based, they are somewhat fragile and not particularly practical for deployment under rugged conditions. The alternative receiver technology cited by [A-6] is Avalanche Photo Diodes (APD). APDs are a solid state device, thus rugged and tolerant of field conditions. However current state-of-the-art APDs are much less sensitive in the solar-blind region. Published literature as far as 2004 [A-5] claims that "orders-of-magnitude advances" in the field of APDs were "just around the corner". In 2008, the University of Virginia did have some success with solar-blind APDs [A-16], but there is still a significant gap between the performance levels of PMTs and APDs (approximately a factor of three difference in sensitivity).

Solar-blind UV emitter technology used in early studies were typically based on UV lasers [A-1] or mercury vapor lamps [A-6]. Neither of these systems is ideal for deployable systems. More recently, UV LEDs developed under the DARPA SUVOS program have been the focus of studies [A-5, A-6, A-10, A-11, A-14]. Arrays of UV LEDs were required in all cases as the optical output power of the UV LEDs is very low (typically 166 µW per LED [A-10]). UV LED arrays sufficient to produce the required power for NLOS systems are large and expensive.

This review indicates that improvements in the area of UV emitter technology will have a significant impact on the state of the art NLOS communications. Plasma-shell-based systems could replace arrays of UV LEDs in a smaller form factor, at a significantly lower cost. This enables higher emitted optical power at levels where current silicon carbide (SiC) APD technology is functional.

References

[A-1]   Junge, D. M., NLOS Electro-optic Laser Communications in the Middle Ultraviolet, Naval Post Graduate School, 1977.

[A-2]   Ross, W.S., An Investigation of Atmospheric Optically Scattered Non-Line-of-Sight Communication Links, Massachusetts Institute of Technology, 1980.

[A-3]   Shaw G. A., Nischan, M., Iyengar, M., Kaushik, S., Griffen, M. K., NLOS UV Communication for Distributed Sensor Systems, MIT Lincoln Laboratory, Lexington, 2000.

[A-4]   Stark, A. M., Ultraviolet Non-Line of Site Digital Communications, Cedarville University, 1995.

[A-5]   Reilly, D. M., Moriarty, D. T., Maynard, J. A., Unique properties of solar blind ultraviolet communication systems for unattended ground sensor networks, BAE Systems North America, Information and Electronic Warfare Systems, 2004.

[A-6]   Shaw, G. A., Seigel, A. M., Model J., Nischan, M., Field Testing and Evaluation of a Solar-Blind UV Communication Link for Unattended Ground Sensors, MIT Lincoln Laboratory, Lexington, MA, 2004.

[A-7]   Shaw, G. A., Seigel, A. M., Nischan, M., Demonstration System and Applications for Compact Wireless Ultraviolet Communications, MIT Lincoln Laboratory, Lexington, MA 02420-9185, 2009.

[A-8]   Xu, Z., Approximate Performance Analysis Of Wireless Ultraviolet Links, Dept. of Electrical Engineering University of California, Riverside, CA 92521, 2007.

[A-9]   Ding, H., Chen, G., Majumdar, A. K., Sadler B. M., Modeling of Non-Line-of-Sight Ultraviolet Scattering Channels for Communication, 2009.

[A-10]   Xu, Z. Sadler, B. M., Topics In Optical Communications, Ultraviolet Communications: Potential And State-Of-The-Art, United States Army Research Laboratory, 2008.

[A-11]   Xu, Z., Chen, G., Abou-Galala, F., Leonardi, M., Experimental performance evaluation of non-line-of-sight ultraviolet communication systems, Department of Electrical Engineering, University of California, Riverside, CA, 2007.

[A-12]   He, Q, Xu, Z., B. Sadler, "Non-Line-Of-Sight Serial Relayed Link For Optical Wireless Communications," Mil. Comms. Conf., 2010.

[A-13]   Ding, H., Xu, Z., Sadler, B. M., A Path Loss Model for Non-Line-of-Sight Ultraviolet Multiple Scattering Channels, Department of Electrical Engineering, University of California, Riverside, CA, Army Research Laboratory, 2010.

[A-14]   Chen, G., Xu, Z., Ding, H., Sadler, B. M., Path loss modeling and performance trade-study for short-range non-line-of-sight ultraviolet communications, Department of Electrical Engineering, University of California, Riverside, CA, U.S. Army Research Laboratory, 2009.

[A-15]   Li, Y., Ning, J., Xu, Z., Krishnamurthy, S. V., UVOC-MAC: A MAC Protocol for Outdoor Ultraviolet Networks, University of California, Riverside, CA, 2010.

[A-16]   Campbell, J. C., Liu, H., Liu, D., McIntosh, D., Bai, X., SiC Avalanche Photodiodes Avalanche Photodiodes, Department of Electrical and Computer Engineering University of Virginia, Charlottesville, VA, 2008.

Appendix B: PMT Sensitivity

Insufficient PMT sensitivity is evident when results in Table 1 from the experimental test setup in Figure 11 are compared to the calculated received photon count rate. LED current is adjusted to hold the

received photon count f_c constant at 2.5 MHz. With low LED forward current, optical power is proportional to current, and discriminator nonlinearity can be ignored for constant count rates. For reference, LED output power is 411 µW at 20 mA, PMT active area is 1.92 cm^2, quantum efficiency QE is 20% at 273 nm.

The expected receiver f_c is calculated for the case of an LED with forward current of 0.60 mA separated from a bare PMT by distance r = 123.1 cm. Emitted optical power P is 12.3 µW, and for a Lambertian emitter, received irradiance I_0 at the PMT is found by solving the equation $P = 2\pi r^2(I_0/\pi)$. In this equation, emitted power P is set equal to the area of a hemisphere with radius r illuminated by irradiance I_0 corrected by a factor of π for the Lambertian distribution. I_0 evaluates to 0.41 nW/cm^2 and multiplying by PMT area provides the incident power on the PMT active area of 0.78 nW. Incident power is converted to photons per second (count rate) by considering the energy of a photon, $E = hc/\lambda$, and reducing incident power by the quantum efficiency. Count rate may be calculated directly by $f_c = QE{\times}P{\times}\lambda/(hc)$, and when evaluated yields 215 MHz, which is in error of the measured 2.5 MHz by a *factor of 86*; received signal strength is 19.3 dB lower than expected.